Receding Horizon Trajectory Optimization for Simultaneous Signal Landscape Mapping and Receiver Localization

Zaher M. Kassas, Jahshan A. Bhatti, and Todd E. Humphreys
The University of Texas at Austin

BIOGRAPHIES

Zaher M. Kassas is a Ph.D. candiate in the Department of Electrical and Computer Engineering at The University of Texas at Austin. He received a B.E. in Electrical Engineering from The Lebanese American University, M.S. in Electrical and Computer Engineering from The Ohio State University, and M.S.E. in Aerospace Engineering from The University of Texas at Austin. He is a member of The University of Texas Radionavigation Laboratory. His research interests include estimation, navigation, autonomous vehicles, control systems, and intelligent transportation.

Jahshan A. Bhatti is a Ph.D. candidate in the Department of Aerospace Engineering and Engineering Mechanics at The University of Texas at Austin. He received a B.S. and M.S.E. in Aerospace Engineering from The University of Texas at Austin. He is a member of The University of Texas Radionavigation Laboratory. His research interests are in the development of small satellites, software-defined radio applications, space weather, and GNSS security and integrity.

Todd E. Humphreys is an assistant professor in the Department of Aerospace Engineering and Engineering Mechanics at The University of Texas at Austin, and Director of The University of Texas Radionavigation Laboratory. He received a B.S. and M.S. in Electrical and Computer Engineering from Utah State University and a Ph.D. in Aerospace Engineering from Cornell University. He specializes in applying optimal estimation and signal processing techniques to problems in radionavigation. His recent focus is on radionavigation robustness and security.

ABSTRACT

A receiver with no *a priori* knowledge about its own states is dropped in an unknown environment comprising multiple signals of opportunity (SOPs) transmitters. Assuming that the receiver could control its maneuvers in the form of acceleration commands, two problems are considered. First, the minimal conditions under which such environment is completely observable are established. It is shown that receiver-controlled maneuvers reduce the minimal required *a priori* information about the environment for complete observability. Second, the trajectories that the receiver should traverse in order to build a high-fidelity signal landscape map of the environment, while simultaneously localizing itself within this map in space and time with high accuracy are prescribed. To this end, the one-step look-ahead (greedy) strategy is compared to the multi-step look-ahead (receding horizon) strategy. The limitations and achieved improvements in the map quality and localization accuracy due to the receding horizon strategy are quantified, and the associated computational burden is discussed.

I. INTRODUCTION

A new navigation paradigm, termed opportunistic navigation (OpNav), has been proposed to improve navigation robustness in Global Navigation Satellite Systems (GNSS)-challenged environments. This paradigm aims to extract positioning and timing information from ambient radio frequency signals of opportunity (SOPs) [1]. OpNav treats all signals as potential SOPs, from conventional GNSS signals to communications signals never intended for use as timing or positioning sources, such as signals from cellular towers and iridium satellites [2, 3]. In collaborative opportunistic navigation (COpNav), multiple OpNav receivers share information to construct and continuously refine a global signal landscape [4].

The OpNav estimation problem is similar to the simultaneous localization and mapping (SLAM) problem in robotics [5, 6]. Both imagine an agent, which starting with incomplete knowledge of its location and surroundings, simultaneously builds a map of its environment and locates itself within that map. In traditional SLAM, the map that gets constructed as the robot moves through the environment is composed of landmarks with associated positions. OpNav extends this concept to radio signals, with SOPs playing the role of landmarks. In contrast to a SLAM environmental map, the OpNav signal landscape is dynamic and more complex. In pseudorange-only OpNav, the receiver must estimate simultaneously with its own states, the states of each SOP, namely the position and velocity of the transmitter, time offset from a reference time base, rate of change of time offset, and a set of parameters that

Preprint of the 2013 ION GNSS Conference Nashville, TN, September 16–20, 2013

characterize the oscillator stability. Metaphorically, the signal landscape map can be thought of as a "jello map," with the jello firmer as the oscillators are more stable.

The observability of COpNav environments comprising multiple receivers with velocity random walk dynamics making pseudorange measurements on multiple SOPs was thoroughly analyzed in [7,8], and the degree of observability, also known as estimability, of the various states was quantified in [9]. While observability is a Boolean property, i.e. it asserts whether a system is observable or not, it does not specify which trajectory is best for information gathering, and consequently estimability. This is the subject of this paper. To this end, the receiver dynamics is modified so to allow for receiver-controlled maneuvers.

Optimizing an observer's path in tracking problems has been studied extensively [10,11]. In such problems, the observer, which has perfect knowledge about its own states, is tracking a mobile target. The trajectory optimization objective is to prescribe trajectories for the observer to maintain good estimates of the target's states. In SLAM, the problem of trajectory optimization is more involved, due to the coupling between the localization accuracy and map quality [12, 13].

Trajectory optimization in OpNav environments can be thought of as a hybrid of: (i) optimizing an observer's path in tracking problems and (ii) optimizing the robot's path in SLAM. First, due to the dynamical nature of the clock error states, the SOP's state space is non-stationary, which makes the problem analogous to tracking non-stationary targets. Second, the similarity to SLAM is due to the coupling between the receiver localization accuracy and signal landscape fidelity. A unique feature of OpNav is that the quality of the estimates not only depends on the spatial trajectory the receiver traverses within the environment, but also depends on the velocity with which the receiver traverses such trajectory [14].

An initial receiver trajectory optimization study was conducted in [14]. The following problem was considered. A receiver with no *a priori* knowledge about its own states is dropped in a planar OpNav environment. Assuming that the receiver could prescribe its own trajectory in the form of velocity commands, what motion planning strategy should the receiver adopt to build a high-fidelity map of the OpNav signal landscape, while simultaneously localizing itself within this map in space and time? To this end, an optimal closed-loop information-theoretic greedy strategy was proposed for receiver motion planning. Three information measures were compared: D-optimality, A-optimality, and E-optimality. It was demonstrated that all such strategies outperformed a receiver moving randomly and in a pre-defined trajectory. Among these measures, the D-optimality outclassed the A-optimality and E-optimality criteria. In [15], it was shown that with proper reformulation, the greedy innovation-based motion planning strategy could be cast into a tractable convex program, the solution of which is computationally efficient and suitable for receivers with limited processing power. Active collaborative signal landscape map building was addressed in [16], and the price of anarchy was assessed, which measures the degradation in the solution quality should the receivers produce their own maps and make their own maneuver decisions versus a completely centralized approach.

This paper's contribution is to extend the work of [14] in two ways. First, it generalizes the receiver dynamics model from a simple first-order model to a second-order model, in which the receiver commands its acceleration. It is shown that the same observability results achieved in [14] still hold even with such higher-order model. In particular, the OpNav environment is fully-observable if and only if the receiver's initial state is known or the initial state of at least one "anchor" SOP is known. Subsequently, in contrast to the findings in [8], it is concluded that a receiver with controlled maneuvers requires less *a priori* knowledge about the OpNav environment for complete observability. The second contribution is to extend the greedy motion planning strategy to a multi-step look-ahead trajectory optimization strategy. It is well-established in the literature that multi-step look-ahead strategies, also known as receding horizon, outperform greedy strategies [13, 17, 18]. However, receding horizon strategies come at the cost of increased computational burden. This paper studies the achieved improvement in the fidelity of the signal landscape map and receiver localization, should the receiver employ receding horizon trajectory optimization instead of the greedy approach. Moreover, the sensitivity of receding horizon strategies to observation noise is studied. It is demonstrated that as the observation noise increases, the receding horizon strategy becomes less effective. Also, the increased computational burden due to receding horizon approaches is discussed.

The remainder of this paper is organized as follows. Section II describes the OpNav environment dynamics and observation model. Section III analyzes various OpNav scenarios and establishes the minimal conditions under which the environment is fully-observable. Section IV formulates the receding horizon receiver trajectory optimization problem. Section V presents simulation results comparing the signal landscape map quality and localization accuracy achieved from the greedy and receding horizon strategies. Concluding remarks are given in Section VI.

II. MODEL DESCRIPTION

A. Dynamics Model

The receiver's dynamics will be assumed to evolve according to the controlled velocity random walk model. An

object moving according to such dynamics in a generic coordinate ξ, has the dynamics

$$\ddot{\xi}(t) = u(t) + \tilde{w}_\xi(t),$$

where $u(t)$ is the control input in the form of acceleration command and $\tilde{w}_\xi(t)$ is a zero-mean white noise process with power spectral density $\tilde{q}_\xi$, i.e.

$$\mathbb{E}\left[\tilde{w}_\xi(t)\right] = 0, \quad \mathbb{E}\left[\tilde{w}_\xi(t)\tilde{w}_\xi(\tau)\right] = \tilde{q}_\xi\, \delta(t-\tau),$$

where $\delta(t)$ is the Dirac delta function. The receiver and SOP clock error dynamics will be modeled according to the two-state model, composed of the clock bias δt and clock drift $\dot{\delta t}$. The clock error states evolve according to

$$\dot{\boldsymbol{x}}_{\text{clk}}(t) = \mathbf{A}_{\text{clk}}\, \boldsymbol{x}_{\text{clk}}(t) + \tilde{\boldsymbol{w}}_{\text{clk}}(t),$$

where

$$\boldsymbol{x}_{\text{clk}} = \begin{bmatrix} \delta t \\ \dot{\delta t} \end{bmatrix}, \quad \tilde{\boldsymbol{w}}_{\text{clk}} = \begin{bmatrix} \tilde{w}_{\delta t} \\ \tilde{w}_{\dot{\delta t}} \end{bmatrix}, \quad \mathbf{A}_{\text{clk}} = \begin{bmatrix} 0 & 1 \\ 0 & 0 \end{bmatrix},$$

where $\tilde{w}_{\delta t}$ and $\tilde{w}_{\dot{\delta t}}$ are modeled as zero-mean, mutually independent white noise processes with power spectra $S_{\tilde{w}_{\delta t}}$ and $S_{\tilde{w}_{\dot{\delta t}}}$, respectively. The power spectra $S_{\tilde{w}_{\delta t}}$ and $S_{\tilde{w}_{\dot{\delta t}}}$ can be related to the power-law coefficients, $\{h_\alpha\}_{\alpha=-2}^{2}$, which have been shown through laboratory experiments to characterize the power spectral density of the fractional frequency deviation $y(t)$ of an oscillator from nominal frequency, namely $S_y(f) = \sum_{\alpha=-2}^{2} h_\alpha f^\alpha$ [19]. It is common to approximate such relationships by considering only the frequency random walk coefficient h_{-2} and the white frequency coefficient h_0, which lead to $S_{\tilde{w}_{\delta t}} \approx \frac{h_0}{2}$ and $S_{\tilde{w}_{\dot{\delta t}}} \approx 2\pi^2 h_{-2}$ [20].

The receiver's state vector will be defined by augmenting the receiver's planar position $\boldsymbol{r}_r$ and velocity $\dot{\boldsymbol{r}}_r$ with its clock error states $\boldsymbol{x}_{\text{clk}}$ to yield the state space realization

$$\dot{\boldsymbol{x}}_r(t) = \mathbf{A}_r\, \boldsymbol{x}_r(t) + \mathbf{B}_r\, \boldsymbol{u}_r(t) + \mathbf{D}_r\, \tilde{\boldsymbol{w}}_r(t), \tag{1}$$

where $\boldsymbol{x}_r = \left[\boldsymbol{r}_r^\mathsf{T},\, \dot{\boldsymbol{r}}_r^\mathsf{T},\, \delta t_r,\, \dot{\delta t}_r\right]^\mathsf{T}$, $\boldsymbol{r}_r = [x_r,\, y_r]^\mathsf{T}$, $\boldsymbol{u}_r = [u_x,\, u_y]^\mathsf{T}$, $\tilde{\boldsymbol{w}}_r = \left[\tilde{w}_x,\, \tilde{w}_y,\, \tilde{w}_{\delta t_r},\, \tilde{w}_{\dot{\delta t}_r}\right]^\mathsf{T}$,

$$\mathbf{A}_r = \begin{bmatrix} \mathbf{0}_{2\times2} & \mathbf{I}_{2\times2} & \mathbf{0}_{2\times2} \\ \mathbf{0}_{2\times2} & \mathbf{0}_{2\times2} & \mathbf{0}_{2\times2} \\ \mathbf{0}_{2\times2} & \mathbf{0}_{2\times2} & \mathbf{A}_{\text{clk}} \end{bmatrix}, \mathbf{B}_r = \begin{bmatrix} \mathbf{0}_{2\times2} \\ \mathbf{I}_{2\times2} \\ \mathbf{0}_{2\times2} \end{bmatrix}, \mathbf{D}_r = \begin{bmatrix} \mathbf{0}_{2\times4} \\ \mathbf{I}_{4\times4} \end{bmatrix}.$$

The receiver's dynamics in (1) is discretized at a constant sampling period $T \triangleq t_{k+1} - t_k$, assuming zero-order hold of the control inputs, i.e. $\{u(t) = u(t_k),\, t_k \le t < t_{k+1}\}$, to yield the discrete-time (DT) model

$$\boldsymbol{x}_r\left(t_{k+1}\right) = \mathbf{F}_r\, \boldsymbol{x}_r(t_k) + \mathbf{G}_r\, \boldsymbol{u}_r(t_k) + \boldsymbol{w}_r(t_k),\ k = 0, 1, 2, \ldots$$

where $\boldsymbol{w}_r$ is a DT zero-mean white noise sequence with covariance $\mathbf{Q}_r = \text{diag}\left[\mathbf{Q}_{\text{pv}},\, \mathbf{Q}_{\text{clk},r}\right]$, with

$$\mathbf{F}_r = \begin{bmatrix} \mathbf{I}_{2\times2} & T\mathbf{I}_{2\times2} & \mathbf{0}_{2\times2} \\ \mathbf{0}_{2\times2} & \mathbf{I}_{2\times2} & \mathbf{0}_{2\times2} \\ \mathbf{0}_{2\times2} & \mathbf{0}_{2\times2} & \mathbf{F}_{\text{clk}} \end{bmatrix}, \mathbf{G}_r = \begin{bmatrix} \frac{T^2}{2}\mathbf{I}_{2\times2} \\ T\,\mathbf{I}_{2\times2} \\ \mathbf{0}_{2\times2} \end{bmatrix}, \mathbf{F}_{\text{clk}} = \begin{bmatrix} 1 & T \\ 0 & 1 \end{bmatrix}$$

$$\mathbf{Q}_{\text{clk},r} = \begin{bmatrix} S_{\tilde{w}_{\delta t_r}} T + S_{\tilde{w}_{\dot{\delta t}_r}} \frac{T^3}{3} & S_{\tilde{w}_{\dot{\delta t}_r}} \frac{T^2}{2} \\ S_{\tilde{w}_{\dot{\delta t}_r}} \frac{T^2}{2} & S_{\tilde{w}_{\dot{\delta t}_r}} T \end{bmatrix}$$

$$\mathbf{Q}_{\text{pv}} = \begin{bmatrix} \tilde{q}_x \frac{T^3}{3} & 0 & \tilde{q}_x \frac{T^2}{2} & 0 \\ 0 & \tilde{q}_y \frac{T^3}{3} & 0 & \tilde{q}_y \frac{T^2}{2} \\ \tilde{q}_x \frac{T^2}{2} & 0 & \tilde{q}_x T & 0 \\ 0 & \tilde{q}_y \frac{T^2}{2} & 0 & \tilde{q}_y T \end{bmatrix}.$$

The SOP will be assumed to emanate from a spatially-stationary terrestrial transmitter, and its state will consist of its planar position and clock error states. Hence, the SOP's dynamics can be described by the state space model

$$\dot{\boldsymbol{x}}_s(t) = \mathbf{A}_s\, \boldsymbol{x}_s(t) + \mathbf{D}_s \tilde{\boldsymbol{w}}_s(t), \tag{2}$$

where $\boldsymbol{x}_s = \left[\boldsymbol{r}_s^\mathsf{T},\, \delta t_s,\, \dot{\delta t}_s\right]^\mathsf{T}$, $\boldsymbol{r}_s = [x_s,\, y_s]^\mathsf{T}$, $\tilde{\boldsymbol{w}}_s = \left[\tilde{w}_{\delta t_s},\, \tilde{w}_{\dot{\delta t}_s}\right]^\mathsf{T}$

$$\mathbf{A}_s = \begin{bmatrix} \mathbf{0}_{2\times2} & \mathbf{0}_{2\times2} \\ \mathbf{0}_{2\times2} & \mathbf{A}_{\text{clk}} \end{bmatrix}, \quad \mathbf{D}_s = \begin{bmatrix} \mathbf{0}_{2\times2} \\ \mathbf{I}_{2\times2} \end{bmatrix}.$$

Discretizing the SOP's dynamics (2) at a sampling interval T yields the DT-equivalent model

$$\boldsymbol{x}_s\left(t_{k+1}\right) = \mathbf{F}_s\, \boldsymbol{x}_s(t_k) + \boldsymbol{w}_s(t_k),$$

where $\boldsymbol{w}_s$ is a DT zero-mean white noise sequence with covariance $\mathbf{Q}_s$, and

$$\mathbf{F}_s = \text{diag}\left[\mathbf{I}_{2\times2},\, \mathbf{F}_{\text{clk}}\right], \quad \mathbf{Q}_s = \text{diag}\left[\mathbf{0}_{2\times2},\, \mathbf{Q}_{\text{clk},s}\right],$$

where $\mathbf{Q}_{\text{clk},s}$ is identical to $\mathbf{Q}_{\text{clk},r}$, except that $S_{\tilde{w}_{\delta t_r}}$ and $S_{\tilde{w}_{\dot{\delta t}_r}}$ are now replaced with SOP-specific spectra, $S_{\tilde{w}_{\delta t_s}}$ and $S_{\tilde{w}_{\dot{\delta t}_s}}$, respectively.

Defining the augmented state as $\boldsymbol{x} \triangleq \left[\boldsymbol{x}_r^\mathsf{T},\, \boldsymbol{x}_s^\mathsf{T}\right]^\mathsf{T}$, the augmented process noise vector as $\boldsymbol{w} \triangleq \left[\boldsymbol{w}_r^\mathsf{T},\, \boldsymbol{w}_s^\mathsf{T}\right]^\mathsf{T}$, and $\boldsymbol{u} \triangleq \boldsymbol{u}_r$, yields the system dynamics

$$\boldsymbol{x}\left(t_{k+1}\right) = \mathbf{F}\, \boldsymbol{x}\left(t_k\right) + \mathbf{G}\, \boldsymbol{u}\left(t_k\right) + \boldsymbol{w}(t_k), \tag{3}$$

where $\mathbf{F} = \text{diag}\left[\mathbf{F}_r,\, \mathbf{F}_s\right]$, $\mathbf{G} = \left[\mathbf{G}_r^\mathsf{T}, \mathbf{0}_{4\times2}^\mathsf{T}\right]^\mathsf{T}$, and $\boldsymbol{w}$ is a zero-mean white noise sequence with covariance $\mathbf{Q} = \text{diag}\left[\mathbf{Q}_r, \mathbf{Q}_s\right]$. While the model defined in (3) considered only one receiver and one SOP, the model can be readily extended to multiple receivers and multiple SOPs by augmenting their corresponding states.

B. Observation Model

To properly model the pseudorange observations, one must consider three different time systems. The first is true time, denoted by the variable t, which can be considered equivalent to Global Positioning System (GPS) time. The second time system is that of the receiver's clock and is denoted t_r. The third time system is that of the SOP's clock and is denoted t_s. The three time systems are related to each other according to

$$t = t_r - \delta t_r(t), \qquad t = t_s - \delta t_s(t),$$

where $\delta t_r(t)$ and $\delta t_s(t)$ represent the amount by which the receiver and SOP clocks are different from true time, respectively.

The pseudorange observation made by the receiver on a particular SOP is made in the receiver time and is modeled according to

$$\begin{aligned}\rho(t_r) = &\\ &\|\boldsymbol{r}_r\left[t_r - \delta t_r(t_r)\right] - \boldsymbol{r}_s\left[t_r - \delta t_r(t_r) - \delta t_{\mathrm{TOF}}\right]\|_2 + \\ &c\,.\,\{\delta t_r(t_r) - \delta t_s\left[t_r - \delta t_r(t_r) - \delta t_{\mathrm{TOF}}\right]\} + \tilde{v}_\rho(t_r), \quad (4)\end{aligned}$$

where c is the speed of light, δt_{TOF} is the time-of-flight of the signal from the SOP to the receiver, and $\tilde{v}_\rho$ is the error in the pseudorange measurement due to modeling and measurement errors. The error $\tilde{v}_\rho$ is modeled as a zero-mean white Gaussian noise process with power spectral density $\tilde{r}$ [21]. In (4), the clock offsets δt_r and δt_s were assumed to be small and slowly changing, in which case $\delta t_r(t) = \delta t_r\left[t_r - \delta t_r(t)\right] \approx \delta t_r(t_r)$. The first term in (4) is the true range between the receiver's position at time of reception and the SOP's position at time-of-transmission of the signal, while the second term arises due to the offsets from true time in the receiver and SOP clocks.

The observation model in (4) can be further simplified by converting it to true time and invoking mild approximations to arrive at [8]

$$\begin{aligned}z(t) = \rho(t) \triangleq h\left[\boldsymbol{x}(t)\right] + \tilde{v}_\rho(t)&\\ \approx \|\boldsymbol{r}_r(t) - \boldsymbol{r}_s(t)\|_2 + c\cdot\left[\delta t_r(t) - \delta t_s(t)\right] + \tilde{v}_\rho(t).& \quad (5)\end{aligned}$$

Discretizing the observation equation (5) at a sampling interval T yields the DT-equivalent model

$$\begin{aligned}z(t_k) = y(t_k) + v_\rho(t_k)& \quad (6)\\ = \|\boldsymbol{r}_r(t_k) - \boldsymbol{r}_s(t_k)\|_2 + c\cdot\left[\delta t_r(t_k) - \delta t_s(t_k)\right] + v_\rho(t_k),&\end{aligned}$$

where v_ρ is a DT zero-mean white Gaussian sequence with covariance $r = \tilde{r}/T$.

III. OBSERVABILITY ANALYSIS

The observability of OpNav environments in which a receiver moved according to velocity random walk dynamics, i.e. without active control over its maneuvers, was considered in [8, 9]. The objective of such observability analysis was twofold: (i) determine the minimal *a priori* knowledge about the environment required for full observability, and (ii) in cases where the environment is not fully-observable, determine the observable states. In this section, the effects of allowing the receiver to actively control its maneuvers on the OpNav environment observability are considered.

A. Theoretical Background: Observability of Nonlinear Systems

For nonlinear systems, it is more appropriate to analyze observability through nonlinear observability tools rather than linearizing the nonlinear system and applying linear observability tools. This is due to two reasons: (i) nonlinear observability tools capture the nonlinearities of the dynamics and observations, and (ii) while the control inputs are never considered in the linear observability tools, they are taken into account in the nonlinear observability tools [22].

For the sake of clarity, the nonlinear observability test employed in this paper is outlined next. Consider the continuous-time (CT) nonlinear dynamic system in the control affine form [23], given by

$$\Sigma_{\mathrm{NL}}: \begin{cases} \dot{\boldsymbol{x}}(t) = \boldsymbol{f}_0\left[\boldsymbol{x}(t)\right] + \sum_{i=1}^{r} \boldsymbol{f}_i\left[\boldsymbol{x}(t)\right] u_i, \quad \boldsymbol{x}(t_0) = \boldsymbol{x}_0 \\ \boldsymbol{y}(t) = \boldsymbol{h}\left[\boldsymbol{x}(t)\right], \end{cases} \quad (7)$$

where $\boldsymbol{x} \in \mathbb{R}^n$ is the system state vector, $\boldsymbol{u} \in \mathbb{R}^r$ is the control input vector, $\boldsymbol{y} \in \mathbb{R}^m$ is the observation vector, and $\boldsymbol{x}_0$ is an arbitrary initial condition.

Several notions of nonlinear observability exist for Σ_{NL} [22]. The most general, is (global) nonlinear observability, in which it might be necessary to travel a considerable distance or for a long period of time to distinguish between initial conditions in $\mathbb{R}^n$. Observability of Σ_{NL} does not imply that every input $\boldsymbol{u}$ distinguishes initial conditions in $\mathbb{R}^n$. Stronger and weaker notions of nonlinear observability exist, namely local observability, weak observability, and local weak observability. A somewhat simple algebraic test exists to assessing local weak observability, which intuitively means that $\boldsymbol{x}_0$ is instantaneously distinguishable from its neighbors. This test is based on constructing the so-called nonlinear observability matrix defined next.

Definition 1. *The first-order Lie derivative of a scalar function h with respect to a vector-valued function $\boldsymbol{f}$ is defined as*

$$\mathfrak{L}^1_{\boldsymbol{f}} h(\boldsymbol{x}) \triangleq \sum_{j=1}^{n} \frac{\partial h(\boldsymbol{x})}{\partial x_j} f_j(\boldsymbol{x}) = \left\langle \nabla_{\boldsymbol{x}} h(\boldsymbol{x}), \boldsymbol{f}(\boldsymbol{x}) \right\rangle, \quad (8)$$

where $\boldsymbol{f}(\boldsymbol{x}) \triangleq [f_1(\boldsymbol{x}), \ldots, f_n(\boldsymbol{x})]^{\mathsf{T}}$. The zeroth-order Lie derivative of any function is the function itself, i.e.

$\mathfrak{L}^0_{\boldsymbol{f}} h(\boldsymbol{x}) = h(\boldsymbol{x})$. *The second-order Lie derivative can be computed recursively as*

$$\mathfrak{L}^2_{\boldsymbol{f}} h(\boldsymbol{x}) = \mathfrak{L}_{\boldsymbol{f}} \left[\mathfrak{L}^1_{\boldsymbol{f}} h(\boldsymbol{x})\right] = \left\langle \left[\nabla_{\boldsymbol{x}} \mathfrak{L}^1_{\boldsymbol{f}} h(\boldsymbol{x})\right], \boldsymbol{f}(\boldsymbol{x}) \right\rangle. \quad (9)$$

Higher-order Lie derivatives can be computed similarly. Mixed-order Lie derivatives of $h(\boldsymbol{x})$ with respect to different functions $\boldsymbol{f}_i$ and $\boldsymbol{f}_j$, given the derivative with respect to $\boldsymbol{f}_i$, can be defined as

$$\mathfrak{L}^2_{\boldsymbol{f}_i \boldsymbol{f}_j} h(\boldsymbol{x}) \triangleq \mathfrak{L}^1_{\boldsymbol{f}_j} \left[\mathfrak{L}^1_{\boldsymbol{f}_i} h(\boldsymbol{x})\right] = \left\langle \left[\nabla_{\boldsymbol{x}} \mathfrak{L}^1_{\boldsymbol{f}_i} h(\boldsymbol{x})\right], \boldsymbol{f}_j(\boldsymbol{x}) \right\rangle.$$

The nonlinear observability matrix, denoted $\boldsymbol{\mathcal{O}}_{\mathrm{NL}}$, of Σ_{NL} defined in (7) is a matrix whose rows are the gradients of Lie derivatives, specifically

$$\boldsymbol{\mathcal{O}}_{\mathrm{NL}} \triangleq \left\{ \nabla^{\mathsf{T}}_{\boldsymbol{x}} \left[\mathfrak{L}^p_{\boldsymbol{f}_i, \ldots, \boldsymbol{f}_j} h_l(\boldsymbol{x})\right] \middle| i, j = 0, \ldots, p;\, p = 0, \ldots, n-1; l = 1, \ldots, m \right\} \quad (10)$$

where $\boldsymbol{h}(\boldsymbol{x}) \triangleq [h_1(\boldsymbol{x}), \ldots, h_m(\boldsymbol{x})]^{\mathsf{T}}$.

The significance of $\boldsymbol{\mathcal{O}}_{\mathrm{NL}}$ is that it can be employed to furnish necessary and sufficient conditions for local weak observability [22, 24]. In particular, if $\boldsymbol{\mathcal{O}}_{\mathrm{NL}}$ is full-rank, then Σ_{NL} is said to satisfy the observability rank condition, in which case the system is locally weakly observable. Moreover, if a system Σ_{NL} is locally weakly observable, then the observability rank condition is satisfied generically. The term "generically" means that the observability matrix is full-rank everywhere, except possibly within a subset of the domain of $\boldsymbol{x}$ [25].

B. Observability Analysis of OpNav Environments

B.1 Scenarios Overview

The various scenarios considered in the observability analysis are outlined Table I, where $m \in \mathbb{N}$. The first scenario corresponds to a single receiver and a single SOP whose initial states are unknown (no *a priori* knowledge about any of the states is available). Subsequent scenarios consider cases of partial or full knowledge of initial states. In Table I, fully-known means that all the initial states are known. Thus, a fully-known receiver is one with known $\boldsymbol{x}_r(t_0)$, whereas a fully-known SOP is one with known $\boldsymbol{x}_s(t_0)$. On the other hand, partially-known means that only the initial position states are known. Thus, a partially-known receiver is one with known $\boldsymbol{r}_r(t_0)$, whereas a partially-known SOP is one with known $\boldsymbol{r}_s(t_0)$. For the cases of multiple SOPs, it is assumed that the SOPs are not colocated at the same position. Moreover, it is assumed that the receiver identifies the SOPs according to their classification: unknown, partially-known, or fully-known.

TABLE I
OpNav observability analysis scenarios considered

Case	Receiver	SOP(s)
1	Unknown	1 Unknown
2	Unknown	m Partially-known
3	Unknown	1 Fully-known
4	Unknown	1 Fully-known & 1 Partially-known
5	Partially-known	1 Unknown
6	Partially-known	m Partially-known
7	Partially-known	1 Fully-known
8	Fully-known	1 Unknown

B.2 Observability Analysis Results

The nonlinear observability test discussed in Subsection III-A was applied to the scenarios outlined in Table I. Table II compares the observable states for the case where the receiver moves according to the controlled velocity random walk dynamics versus the uncontrolled velocity random walk dynamics. It is concluded that adding inputs reduces the *a priori* knowledge needed for observability of the OpNav environment. This conclusion is captured in the following theorem.

Theorem 1. *A planar OpNav environment comprising a receiver moving according to velocity random walk dynamics making pseudorange observations on m terrestrial stationary SOPs is fully-observable if and only if the initial states of at least: (i) the receiver is fully-known, (ii) the receiver is partially-known and one SOP is fully-known, or (iii) one SOP is fully-known and one SOP is partially-known. If the receiver controls its maneuvers in the form of acceleration commands, the environment is fully-observable if and only if the initial states of at least: (i) the receiver is fully-known or (ii) one SOP is fully-known.*

TABLE II
OpNav observability analysis results: Observable states

Case	Without Control	With Control
1	none	$\dot{x}_r$, $\dot{y}_r$
2	$m = 1$: none $m \geq 2$: x_r, y_r, $\dot{x}_r$, $\dot{y}_r$	$m \geq 1$: x_r, y_r, $\dot{x}_r$, $\dot{y}_r$
3	δt_r, $\dot{\delta} t_r$	all
4	all	all
5	$\dot{x}_r$, $\dot{y}_r$, x_s, y_s	$\dot{x}_r$, $\dot{y}_r$, x_s, y_s
6	$\dot{x}_r$, $\dot{y}_r$	$\dot{x}_r$, $\dot{y}_r$
7	all	all
8	all	all

IV. RECEDING HORIZON RECEIVER TRAJECTORY OPTIMIZATION

The proposed receding horizon trajectory optimization loop is illustrated in Fig. 1. At a particular time-step t_k, the pseudorange observations made by the receiver on the SOPs in the environment, $\boldsymbol{z}(t_k) \triangleq [z_1(t_k), \ldots, z_m(t_k)]^{\mathsf{T}}$, are fused through an estimator, an extended Kalman filter (EKF) in this case, which produces state estimate $\hat{\boldsymbol{x}}(t_k|t_k)$ and associated estimation error covariance $\mathbf{P}(t_k|t_k)$. The estimate and associated covariance are fed into a Receding Horizon Optimal Control block, which solves for the optimal admissible N-step look-ahead control actions $\left(\boldsymbol{U}_{t_k}^{N}\right)^{\star} \triangleq \{\boldsymbol{u}^{\star}(t_{k+N-j}),\, j = 1, \ldots, N\}$. In Fig. 1, $v_{r,\max}$ and $a_{r,\max}$ represent the maximum speed and acceleration, respectively, with which the receiver can move.

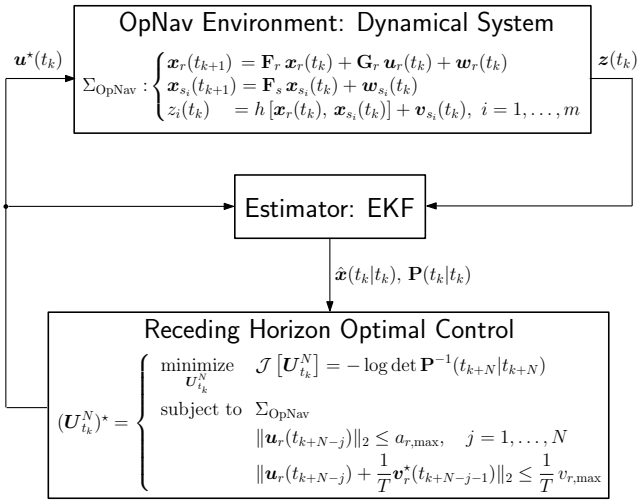

Fig. 1. Receding horizon receiver motion planning loop

Note that if $N = 1$, the receding horizon trajectory optimization problem reduces to greedy optimization. The cost functional $\mathcal{J}$ was chosen as the D-optimality criterion, which was demonstrated in [14] to be superior to the A-optimality and E-optimality criteria. To evaluate the N-step estimation error covariance, $\mathbf{P}(t_{k+N}|t_{k+N})$, the zero future innovations assumption, namely $\tilde{\boldsymbol{z}}(t_{j+1}) = \boldsymbol{z}(t_{j+1}) - \boldsymbol{h}\,[\hat{\boldsymbol{x}}(t_{j+1}|t_j)] \equiv 0$, for $j = k, \ldots, k+N-1$, will be invoked [13, 17]. Once the optimal N-step look-ahead control actions $\left(\boldsymbol{U}_{t_k}^{N}\right)^{\star}$ are found, only the first control action $\boldsymbol{u}^{\star}(t_k)$ is applied, whereas the rest of the control actions are discarded. At the next time-step, t_{k+1}, a new measurement becomes available, which contains information that will be utilized to refine the optimal trajectory by repeating the same procedure. A single iteration of the algorithm for finding the receding horizon optimal receiver trajectory is outline in Algorithm 1.

The main drawback of receding horizon trajectory optimization methods is increased computational burden. Fig. 2 illustrates the cascade of feasibility regions that should be considered as the horizon is increased. In particular, each point in the black shaded region corresponding to the feasibility region of the first-step look-ahead has an associated feasibility region of its own signifying the feasible maneuvers the receiver could take for the second-step. The number of optimization variables for an N-step look-ahead problem are $2N$. Denoting the number of feasible maneuvers in a particular time-step t_j by n_j, it is easy to see that an exhaustive search-type algorithm has a computational burden $\mathcal{O}\left(\prod_{j=1}^{N} n_j\right)$.

Algorithm 1 Receding horizon trajectory optimization

Given: $\hat{\boldsymbol{x}}(t_k|t_k)$, $\mathbf{P}(t_k|t_k)$, N
for $j = k, \ldots, k+N-1$ **find**
$\hat{\boldsymbol{x}}(t_{j+1}|t_j) = \mathbf{F}\hat{\boldsymbol{x}}(t_j|t_j) + \mathbf{G}\boldsymbol{u}(t_j)$
$\mathbf{H}(t_{j+1}) = \left.\frac{\partial \boldsymbol{h}[\boldsymbol{x}_r(t_{j+1}),\, \boldsymbol{x}_s(t_{j+1})]}{\partial \boldsymbol{x}}\right|_{\boldsymbol{x}=\hat{\boldsymbol{x}}(t_{j+1}|t_j)}$
$\mathbf{P}(t_{j+1}|t_j) = \mathbf{F}\mathbf{P}(t_j|t_j)\mathbf{F}^{\mathsf{T}} + \mathbf{Q}$
$\mathbf{S}(t_{j+1}) = \mathbf{H}(t_{j+1})\mathbf{P}(t_{j+1}|t_j)\mathbf{H}^{\mathsf{T}}(t_{j+1}) + \mathbf{R}$
$\mathbf{W}(t_{j+1}) = \mathbf{P}(t_{j+1}|t_j)\mathbf{H}^{\mathsf{T}}(t_{j+1})\mathbf{S}^{-1}(t_{j+1})$
$\mathbf{P}(t_{j+1}|t_{j+1}) = \mathbf{P}(t_{j+1}|t_j) - \mathbf{W}(t_{j+1})\mathbf{S}(t_{j+1})\mathbf{W}^{\mathsf{T}}(t_{j+1})$
$\hat{\boldsymbol{x}}(t_{j+1}|t_{j+1}) \equiv \hat{\boldsymbol{x}}(t_{j+1}|t_j)$
end for
Solve:
$\underset{\boldsymbol{U}_{t_k}^{N}}{\text{minimize}} \quad \mathcal{J}\left[\boldsymbol{U}_{t_k}^{N}\right] = -\log\det\mathbf{P}^{-1}(t_{k+N}|t_{k+N})$
subject to Σ_{OpNav}
$\|\boldsymbol{u}_r(t_{k+N-j})\|_2 \le a_{r,\max},\quad j = 1, \ldots, N$
$\left\|\boldsymbol{u}_r(t_{k+N-j}) + \frac{\boldsymbol{v}_r^{\star}(t_{k+N-j-1})}{T}\right\|_2 \le \frac{v_{r,\max}}{T}$
Apply: $\boldsymbol{u}^{\star}(t_k)$
Discard: $\{\boldsymbol{u}^{\star}(t_{k+1}), \ldots, \boldsymbol{u}^{\star}(t_{k+N-1})\}$

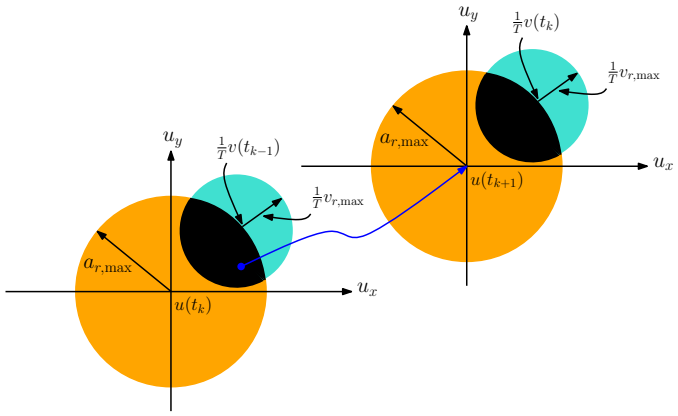

Fig. 2. Feasibility regions for two-step look-ahead horizon

V. SIMULATION RESULTS

This section presents simulation results to demonstrate the limitations and effectiveness of the receding horizon trajectory optimization method versus the greedy approach. An OpNav environment comprising a receiver,

one known "anchor" SOP, and three unknown SOPs was simulated according to the settings presented in Table III. The receiver's and SOPs' clocks were assumed to be temperature-compensated and oven-controlled crystal oscillators (TCXOs and OCXOs), respectively. For purposes of numerical stability, the clock error states were defined to be $c\delta t$ and $c\dot{\delta t}$. Four receiver trajectories were generated: a random trajectory, a greedy trajectory, and two receding horizon trajectories with $N = 2$ and $N = 3$.

TABLE III
SIMULATION SETTINGS

Parameter	Value
$\boldsymbol{x}_r(t_0)$	$[0,\ 0,\ 10,\ 0,\ 100,\ 10]^\mathsf{T}$
$\boldsymbol{x}_{s_1}(t_0)$	$[0,\ 150,\ 10,\ 0.1]^\mathsf{T}$
$\boldsymbol{x}_{s_2}(t_0)$	$[100,\ -150,\ 20,\ 0.2]^\mathsf{T}$
$\boldsymbol{x}_{s_3}(t_0)$	$[200,\ 200,\ 30,\ 0.3]^\mathsf{T}$
$\boldsymbol{x}_{s_4}(t_0)$	$[-150,\ 50,\ 40,\ 0.4]^\mathsf{T}$
$\hat{\boldsymbol{x}}_r(t_0\|t_0)$	$\sim \mathcal{N}\left[\boldsymbol{x}_r(t_0), \mathbf{P}_r(t_0\|t_0)\right]$
$\hat{\boldsymbol{x}}_{s_i}(t_0\|t_0)$	$\sim \mathcal{N}\left[\boldsymbol{x}_{s_i}(t_0), \mathbf{P}_{s_i}(t_0\|t_0)\right],\ i = 2,3,4$
$\mathbf{P}_r(t_0\|t_0)$	$(10^4) \cdot \mathrm{diag}\left[1,1,1,1,1,10^{-2}\right]$
$\mathbf{P}_{s_i}(t_0\|t_0)$	$(10^4) \cdot \mathrm{diag}\left[1,1,1,10^{-2}\right],\ i = 2,3,4$
$\{h_{0,r},\ h_{-2,r}\}$	$\{2 \times 10^{-19},\ 2 \times 10^{-20}\}$
$\{h_{0,s_j},\ h_{-2,s_j}\}$	$\{8 \times 10^{-20},\ 4 \times 10^{-23}\}, j = 1,\ldots,4$
$\tilde{q}_x, \tilde{q}_y$	$0.1\,(\mathrm{m/s}^3)^2$
r	$\{250,\ 300,\ 350\}\ \mathrm{m}^2$
$\{v_{\max},\ a_{\max}\}$	$\{10\,\mathrm{m/s},\ 3\,\mathrm{m/s}^2\}$
T	$0.2\,\mathrm{s}$

To assess the localization accuracy and signal landscape map quality, the natural logarithm of the posterior estimation error covariance, namely $\log\det\left[\mathbf{P}(t_{k+1}|t_{k+1})\right]$, was adopted. Such metric is proportional to the volume of the estimation error uncertainty ellipsoid [14]. Three sets of simulations were performed for three different observation noise intensities, specifically $r \in \{250,\ 300,\ 350\}\ \mathrm{m}^2$.

The resulting receiver trajectories for $r = 250\,\mathrm{m}^2$ are illustrated in Fig. 3. The resulting localization and signal landscape map uncertainties for $r \in \{250,\ 300,\ 350\}\ \mathrm{m}^2$ are plotted in Fig. 4-6. The reduction in receiver localization and signal landscape map estimation uncertainty for the receding horizon approaches over the greedy approach at the end of the simulation time is tabulated in Table IV. The following conclusions can be drawn from the presented simulations. First, greedy motion planning and receding horizon trajectory optimization yielded superior results to random trajectories. Second, receding horizon trajectory optimization outperformed greedy motion planning. Third, the superiority of receding horizon over greedy motion planning depends on the observation noise intensity – the larger the observation noise, the less effective the receding horizon strategy becomes. In fact, for large enough observation noise, receding horizon could yield identical (or worse) performance than greedy.

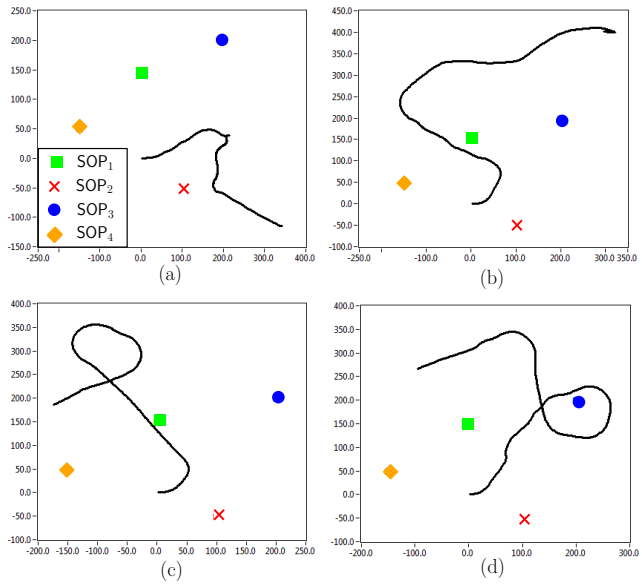

Fig. 3. Receiver trajectories due to (a) random motion, (b) optimal greedy motion, (c) optimal two-step look-ahead motion, and (d) optimal three-step look ahead motion

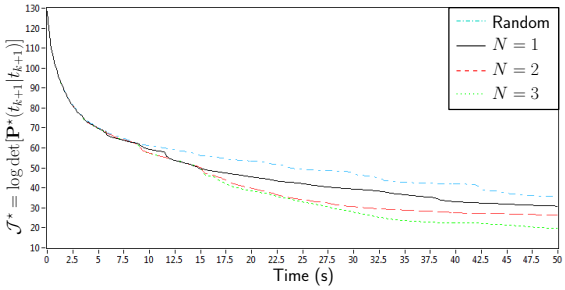

Fig. 4. Localization & signal landscape map uncertainty for $r = 250$

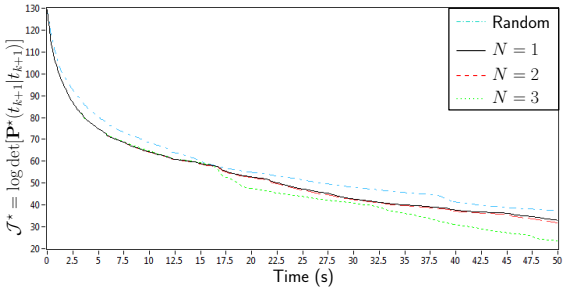

Fig. 5. Localization & signal landscape map uncertainty for $r = 300$

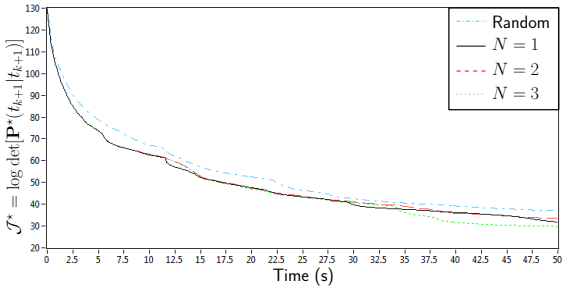

Fig. 6. Localization & signal landscape map uncertainty for $r = 350$

TABLE IV

% Reduction in receiver localization and signal landscape map estimation uncertainty for the receding horizon approaches over the greedy approach

N	$r = 250$	$r = 300$	$r = 350$
2	14.08	3.32	-4.81
3	36.54	28.43	10.75

VI. CONCLUSIONS

This paper studied the problem of multi-step look-ahead (receding horizon) receiver trajectory optimization for simultaneous signal landscape map building and receiver localization. To this end, it was first shown that the minimal observability conditions for a planar environment comprising a receiver moving according to controlled velocity random walk dynamics making pseudorange observations on multiple terrestrial SOPs are identical to the minimal conditions established for a receiver moving according to controlled position random walk dynamics. In particular, the environment is fully-observable if and only the initial state of the receiver is fully-known or the initial state of at least one anchor SOP is fully-known. Furthermore, random receiver trajectories, greedy motion planning, and receding horizon strategies were compared. It was demonstrated that optimal greedy and receding horizon receiver motion planning resulted in higher fidelity signal landscape maps and more accurate receiver localization than random receiver trajectories. Moreover, it was demonstrated that while the receding horizon strategy outperformed the greedy method, the receding horizon strategy became less effective as the observation noise intensity was increased.

References

[1] K. Pesyna, Z. Kassas, J. Bhatti, and T. Humphreys, "Tightly-coupled opportunistic navigation for deep urban and indoor positioning," in *Proceedings of the ION GNSS*, vol. 1, September 2011, pp. 3605–3617.

[2] C. Yang, T. Nguyen, E. Blasch, and D. Qiu, "Assessing terrestrial wireless communications and broadcast signals as signals of opportunity for positioning and navigation," in *Proceedings of the ION GNSS*, September 2012, pp. 3814–3824.

[3] K. Pesyna, Z. Kassas, and T. Humphreys, "Constructing a continuous phase time history from TDMA signals for opportunistic navigation," in *Proceedings of IEEE/ION Position Location and Navigation Symposium*, April 2012, pp. 1209–1220.

[4] Z. Kassas, "Collaborative opportunistic navigation," *IEEE Aerospace and Electronic Systems Magazine*, vol. 28, no. 6, pp. 38–41, June 2013.

[5] H. Durrant-Whyte and T. Bailey, "Simultaneous localization and mapping: part I," *IEEE Robotics and Automation Magazine*, vol. 13, no. 2, pp. 99–110, June 2006.

[6] T. Bailey and H. Durrant-Whyte, "Simultaneous localization and mapping: part II," *IEEE Robotics and Automation Magazine*, vol. 13, no. 3, pp. 108–117, September 2006.

[7] Z. Kassas and T. Humphreys, "Observability analysis of opportunistic navigation with pseudorange measurements," in *Proceedings of AIAA Guidance, Navigation, and Control Conference*, vol. 1, August 2012, pp. 4760–4775.

[8] ——, "Observability analysis of collaborative opportunistic navigation with pseudorange measurements," *IEEE Transactions on Intelligent Transportation Systems*, 2013, in press.

[9] ——, "Observability and estimability of collaborative opportunistic navigation with pseudorange measurements," in *Proceedings of the ION GNSS*, September 2012, pp. 621–630.

[10] Y. Oshman and P. Davidson, "Optimization of observer trajectories for bearings-only target localization," *IEEE Transactions on Aerospace and Electronic Systems*, vol. 35, no. 3, pp. 892–902, July 1999.

[11] S. Ponda, R. Kolacinski, and E. Frazzoli, "Trajectory optimization for target localization using small unmanned aerial vehicles," in *Proceedings of AIAA Guidance, Navigation, and Control Conference*, August 2009, pp. 1209–1220.

[12] H. Feder, J. Leonard, and C. Smith, "Adaptive mobile robot navigation and mapping," *International Journal of Robotics Research*, vol. 18, no. 7, pp. 650–668, July 1999.

[13] C. Leung, S. Huang, N. Kwok, and G. Dissanayake, "Planning under uncertainty using model predictive control for information gathering," *Robotics and Autonomous Systems*, vol. 54, no. 11, pp. 898–910, November 2006.

[14] Z. Kassas and T. Humphreys, "Motion planning for optimal information gathering in opportunistic navigation systems," in *Proceedings of AIAA Guidance, Navigation, and Control Conference*, August 2013, pp. 4551–4565.

[15] ——, "Greedy motion planning for simultaneous signal landscape mapping and receiver localization," *IEEE Transactions on Aerospace and Electronic Systems*, 2013, under review.

[16] ——, "The price of anarchy in active signal landscape map building," in *Proceedings of IEEE Global Conference on Signal and Information Processing*, December 2013.

[17] S. Huang, N. Kwok, G. Dissanayake, Q. Ha, and G. Fang, "Multi-step look-ahead trajectory planning in SLAM: Possibility and necessity," in *Proceedings of IEEE International Conference on Robotics and Automation*, April 2005, pp. 1091–1096.

[18] G. Lidoris, K. Kuhnlenz, D. Wollherr, and M. Buss, "Combined trajectory planning and gaze direction control for robotic exploration," in *Proceedings IEEE International Conference on Robotics and Automation*, April 2007, pp. 4044–4049.

[19] A. Thompson, J. Moran, and G. Swenson, *Interferometry and Synthesis in Radio Astronomy*, 2nd ed. John Wiley & Sons, 2001.

[20] Y. Bar-Shalom, X. Li, and T. Kirubarajan, *Estimation with Applications to Tracking and Navigation*, 1st ed. New York, NY: John Wiley & Sons, 2002.

[21] M. Psiaki and S. Mohiuddin, "Modeling, analysis, and simulation of GPS carrier phase for spacecraft relative navigation," *Journal of Guidance, Control, and Dynamics*, vol. 30, no. 6, pp. 1628–1639, November-December 2007.

[22] R. Hermann and A. Krener, "Nonlinear controllability and observability," *IEEE Transactions on Automatic Control*, vol. 22, no. 5, pp. 728–740, October 1977.

[23] M. Anguelova, "Observability and identifiability of nonlinear systems with applications in biology," Ph.D. dissertation, Chalmers University Of Technology and Göteborg University, Sweden, 2007.

[24] W. Respondek, "Geometry of static and dynamic feedback," in *Lecture Notes at the Summer School on Mathematical Control Theory*, Trieste, Italy, September 2001.

[25] J. Casti, "Recent developments and future perspectives in nonlinear system theory," *SIAM Review*, vol. 24, no. 3, pp. 301–331, July 1982.